Equivalent Thermal Conductivity Prediction of Form-Wound Windings with Litz Wire Considering Transposition Effect

Xuan Yi
Dept. of Elec. and Comp. Engr
Univ. of Illinois Urbana-Champaign
Urbana, IL, U.S.
xuanyi2@illinois.edu

Xiaojian Qiao
Dept. of Elec. and Comp. Engr
Univ. of Illinois Urbana-Champaign
Urbana, IL, U.S.
jxiao14@illinois.edu

Tianyu Yang
Dept. of Mech. Engr
Univ. of Illinois Urbana-Champaign
Urbana, IL, U.S.
tianyuy2@illinois.edu

Kiruba S. Haran
Dept. of Elec. and Comp. Engr
Univ. of Illinois Urbana-Champaign
Urbana, IL, U.S.
kharan@illinois.edu

Nenad Miljkovic
Dept. of Mech. Engr
Univ. of Illinois Urbana-Champaign
Urbana, IL, U.S.
nmiljkov@illinois.edu

***Abstract*—Litz wire has been widely used in high-frequency electrical machines and transformers to minimize induced current loss and maintain high efficiency. Its heat dissipation capability can be a key design factor for high-power-density electrical machine and power electronics. Although litz wire equivalent thermal conductivity has been studied, its transposition effect is usually ignored. This paper focus on developing an analytical model to predict litz wire equivalent thermal conductivity considering its bundle transposition effects. A 3-D litz wire is modeled and simulated to validate analytical results. Also, transposed and parallel arrangement effects on litz wire equivalent thermal conductivity are compared and discussed. Hardware experiments are used to validate the analytical results in the end. The predictions of using the proposed analytical model match up well with both simulation and experimental results.**

***Index Terms*—litz wire, composite,thermal conductivity, electrical machine**

I. Introduction

As hybridization and electrification of vehicle and airplane powertrain increase to meet power density, efficiency and emissions requirements, thermal design becomes a critical enabling factor [1]. The machine hotspot temperature determines allowable electric loading within insulation capability, and directly impacts torque density and power density [2]. Therefore, thermal managment of stator winding needs to be studied first to enable high-power-density and high-efficiency electrical machine [3].

Litz wire is often selected for high-power-density and high-efficiency electrical machines and power converters, since it significantly reduces eddy-current loss with smaller conductor size and transposition arrangement [4] [5]. However, with various insulation layers (of strands, bundles, and turns) and potting materials, stator winding block becomes a complex composite. Modeling stator winding with detailed small strands, transposition arrangement, and different insulation layers, becomes a challenging and time-consuming process for machine design process. Fast but accurate prediction of winding composite effective thermal conductivity is desired for multi-physics machine design optimization [6].

Most of winding equivalent thermal conductivity analytical studies focus on the parallel arrangement. All of strands and bundles are in parallel. Detailed 2-D finite-element-analysis (FEA) can be conducted for accurate prediction [3], [7], [8]. For fast estimation, homogenization techniques are used to predict winding thermal equivalent conductivity by regrouping copper, insulation and resin areas [9], [10], [11] . A more accurate approach is using multi-scales method to account for wire shape and distribution spacing effect [12]. However, few literature considers transposition effects in litz wire configuration. [10] studied litz wire equivalent thermal conductivity by neglecting bundle transposition effects. [13] presented a thermal equivalent circuit of litz wire considering transposed effect. But it does not provide any analytical solution for predicting transposed litz wire.

This paper takes the challenge of developing an analytical model to predict equivalent thermal conductivity of litz wire considering transposition effects. The presented model has advantages of less computational time and good accuracy compared finite-element method. And it can be easily integrated in machine design process to optimize winding dimension and strand selection by coupling electromagnetic and thermal analysis. This analytical model is validated with 3-D FEA simulation and hardware experiment. The analytical prediction results show good agreement with both simulation

This work was supported by the National Science Foundation Engineering Research Center for Power Optimization of Electro Thermal Systems (POETS) and NASA Glenn Research Center.

978-1-5386-9350-6/19/$31.00 ©2019 IEEE

(a) Staggered Winding

(b) Selected Rectangular Transposed Litz Wire

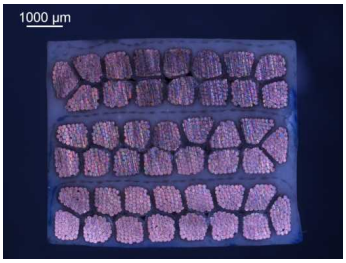

(c) Strands and Bundles within Litz Wire(Credit: NASA Glenn Research Center)

Fig. 1: Litz Wire Model Sample

and hardware results. Also, in the simulation, transposition arrangement litz wire indicates enhancement of heat dissipation compared with parallel arrangement one. This advantage could play a critical role in high-power-density, and high-efficiency electrical machines and power electronics design. Therefore, transposition effects of litz wire are worth being studied in more details while most of papers ignore.

II. Transposed Litz Wire Geometry and Materials

The Litz wire used in this paper is selected in a high-frequency high-specific MW-level slotless machine [14]. It consists of 660 AWG 38 strands separated into 15 bundles as shown in Fig. 1b.The selected litz wire maintains rectangular shape of 0.244" by 0.063".

TABLE I: Thermal Properties of Winding Materials

	Type	Thick(mil)	Max Temp(C)	Thermal Cond.(W/mK)
Strand	Polymide	1	240	0.1
Bundle	Nomex	5	220	0.1
Resin	Duraco 128		260	1.7

Each strand surface is brushed with heavy polymide coating. Forty-four strands form a bundle wrapped with polymide insulation, which has the lowest material temperature limit in the whole machine. This strand size and wire arrangements are selected to minimize induced current loss while maintaining decent fill factor and electric loading. Epoxy resin was employed to firmly bundle Litz wires in specifically designed slot geometries shown in Fig. 1a. The associated thermal conductivity properties are presented in Table I.

III. Equivalent Thermal Conductivity Analytical Analysis

The section focus on finding equivalent thermal conductivity across the rectangular litz wire cured with epoxy resin shown in Section II. Homogenization within bundles need to be adopted first. The potted litz wire effective thermal conductivity is then evaluated with an analytical model considering transposition effects. Both general and simplified model were derived.

A. Homogenization within Bundles

Since each bundle of the selected litz wire contains numerous small strands, strand /bundle insulation, and resin, homogenization needs to be applied to find its effective thermal conductivity. The detailed litz wire cross section view is presented in Fig. 1c. The first step is to find the effective thermal conductivity of strand. In this case, strand has a circle shape with strand insulation coating. It is still treated as a square shape for calculation simplification. Then, the corresponding prediction equations are

$$k_{s,II} = (r_s + t_s) \cdot \left(\frac{r_s}{k_{cu}} + \frac{t_s}{k_{ins}} \right)^{-1} \tag{1}$$

$$k_{strand,r} = \frac{2k_{ins}t_s + k_{s,II}}{2(t_s + r_s)} \tag{2}$$

where r_s and t_s are strand radius and insulation thickness, k_{cu} and k_{ins} are copper and insulation thermal conductivity.

The next step is to evaluate bundle effective thermal conductivity. According to [11], the bundle equivalent thermal conductivity along with radial (perpendicular) direction can be evaluated by

$$k_{bundle,r} = k_{res} \frac{(1+ff)k_{strand,r} + (1-ff)k_{res}}{(1-ff)k_{strand,r} + (1+ff)k_{res}} \tag{3}$$

where k_{res} and $k_{strand,r}$ are thermal conductivity of filled resin and strand along perpendicular direction, ff is fill factor of conductor within homogenization area. If bundle has a layer of insulator, (3) needs to be fed into (1) and (2) to get correction to include bundle insulation thermal effect.

B. Homogenization within Litz Wire Considering Transposition Effect

The selected litz wire consists of two layers of bundles. These two layers of bundles are wrapped together to form a rectangular wire shape with a transposition angle of θ, 23.78 degree. The detailed geometry modeling is presented in Fig. 2.

There are mainly two heat flow paths of each bundle considered in this analytical model as shown in Fig. 3. One is along the bundle radial (perpendicular) direction. The other

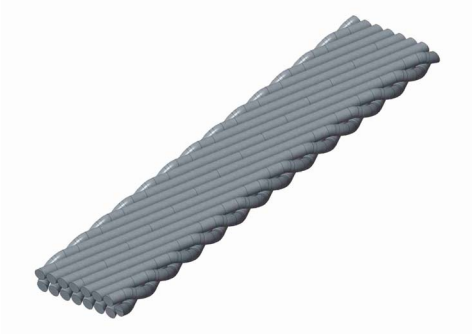

Fig. 2: One Pitch Litz Wire Geometry - Full Model

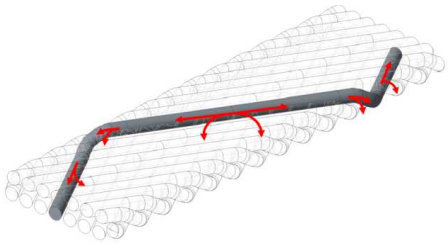

Fig. 3: One Pitch Litz Wire Geometry of Single Bundle with Heat Path Flow Arrows in Radial and Axial Directions

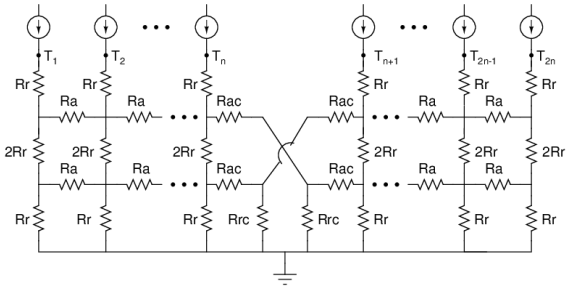

Fig. 4: General Thermal Equivalent Circuit of the Selected Bundle within Half Pitch

one is the bundle axial (transverse) direction. Both paths are interleaved each other to extract heat from winding. The axial heat path of bundles are ignored over here, since the main heat dissipation path of winding in electrical machines is along with radial direction of bundles in litz wire.

1) Generalized Model: The proposed analytical model focus on two symmetrical bundles within cured litz wires. These two bundles are decomposed into small lumped component including both radial and axial thermal resistances. And these two bundles are interleaved each other to form a meshed lumped equivalent circuit as in Fig. 4. Heat source is modeled as current source and injected on the top of each bundle. The node temperature rise on the bundle top surface can be obtained by solving the proposed equivalent circuit by the following analytical method. It can be implemented in MATLAB or other mathematical calculation programming tools. The temperature rise is not uniform in this case, although a uniform heat flux boundary condition is imposed on the top of winding surface. This is due to non-uniform thermal resistances and heat dissipation path lengths. Also, this general model only analyzes one turn or layer of winding. The axial length is assumed to be half pitch because of the repeating geometry pattern.

The modeled litz wire section is decomposed into four and $2n$ layers along with radial and axial direction respectively. R_{ac} and R_{rc} are the lumped thermal resisrance of curve part. The radial and axial thermal resistances in the equivalent circuit of Fig. 4 and 5 are

$$R_r = \frac{n \cdot H}{W(L\sec\theta - 2H\csc\theta)} \frac{k_f}{k_{b,r}} \frac{(1+ff)k_{b,r} + (1-ff)k_f}{(1-ff)k_{b,r} + (1+ff)k_f} \tag{4}$$

$$R_a = \frac{L\sec\theta - 2H\csc\theta}{n \cdot WHk_{b,a} \cdot ff} \tag{5}$$

$$R_{rc} = \frac{\cos\theta}{W} \frac{k_f}{k_{b,r}} \frac{(1+ff)k_{b,r} + (1-ff)k_f}{(1-ff)k_{b,r} + (1+ff)k_f} \tag{6}$$

$$R_{ac} = \frac{\csc\theta}{Wk_{b,a} \cdot ff} + R_a \tag{7}$$

where ff is the bundle area fill factor of wire cross section, L, H, W are the litz wire one pitch rectangular dimensions, $k_{b,r}$ and $k_{b,a}$ are bundle equivalent thermal conductivity, θ is transposed angle.

The proposed lumped mesh circuit model can be solved analytically by using iterative method to eliminate intersection nodes of three or four branches. The goal of solving this meshing circuit is to find equivalent resistance associated with each current source by eliminating mesh intersection nodes. Such elimination process starts from the edge of circuit and propagates towards the source-associated branch.

Suppose T_1 is the unknown target shown in Fig. 5. Only the heat source at branch 1 is active, and other heat sources are open by the superposition principle. The circuit simplification starts from the branch $2n$ and $2n-1$. There will be two Y-delta transformations to remove meshing circuit intersections of branch $2n$. The transformation process can be applied to each branch iteratively.

The first transformation is shown in Fig. 6. Basically, the intersection point highlighted as blue in Fig. 6 is the elimination target. The associated resistances are given as:

$$R_t = 2R_r, \quad R_m = R_a, \quad R_b = R_r; \tag{8}$$

$$R'_{d\_tm} = \frac{R_tR_m + R_mR_b + R_tR_b}{R_b} \tag{9}$$

$$R'_{d\_mb} = \frac{R_tR_m + R_mR_b + R_tR_b}{R_t} \tag{10}$$

$$R'_{d\_tb} = \frac{R_tR_m + R_mR_b + R_tR_b}{R_m} \tag{11}$$

where t denotes as top, m denotes as middle, and b denotes as bottom.

Then, the next step is to remove the highlighted red intersection point in Fig. 7. The first transformation results need to be grouped into the branch $2n-1$ and manipulated as 7

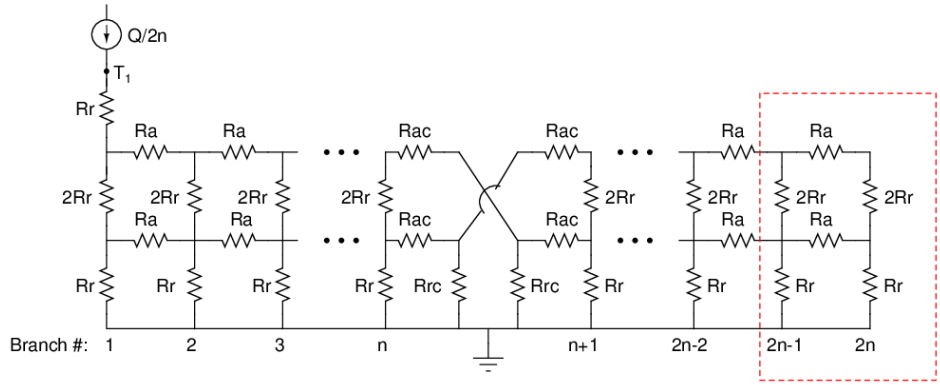

Fig. 5: General Thermal Equivalent Circuit Seen at the Branch #1 Heat Source Injection Point

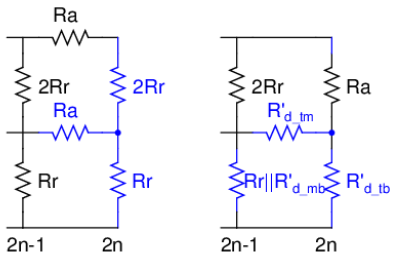

Fig. 6: First Circuit Transformation within Branch #2n-1 and #2n

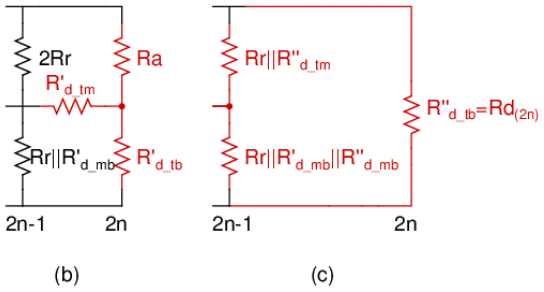

Fig. 7: Second Circuit Transformation within Branch #2n-1 and #2n

(b). The associated resistances of the second transformation can be obtained as:

$$R''_{d\_tm} = \frac{R_a R'_{d\_tm} + R_a R'_{d\_tb} + R'_{d\_tm} R'_{d\_tb}}{R'_{d\_tb}} \quad (12)$$

$$R''_{d\_mb} = \frac{R_a R'_{d\_tm} + R_a R'_{d\_tb} + R'_{d\_tm} R'_{d\_tb}}{R_a} \quad (13)$$

$$R''_{d\_tb} = \frac{R_a R'_{d\_tm} + R_a R'_{d\_tb} + R'_{d\_tm} R'_{d\_tb}}{R'_{d\_tm}} \quad (14)$$

$$R_{d(2n)} = R''_{d\_tb} \quad (15)$$

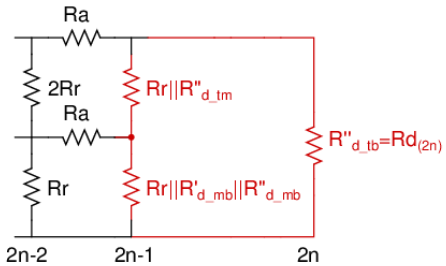

Fig. 8: Circuit Simplification of Branch #2n-1 and #2n

With the above two Y-delta transformations, the branch n only has one resistor $R_{d(2n)}$ in parallel with other branches shown in Fig. 8 (d). And the branch $2n-1$ results into the same circuit structure of 6 (a). The exact calculation process can be conducted through the branch $2n-2$ and $2n-1$ with (7)-(14). The only change in this process is to update R_t, R_m, and R_b with transformed resistor values shown as

$$R_t = R_r || R''_{d\_tm}, \quad R_m = R_a, \quad R_b = R_r || R'_{d\_mb} || R''_{d\_mb}; \quad (16)$$

An iterative method can be used to calculate equivalent resistor in each branch following the above transformation procedure. After going through all of the branches from $2n$ to 1, there will be only one equivalent resistance associated with each branch. That means there are $2n$ parallel resistors resulting from the mesh intersection elimination process. Therefore, the total equivalent resistance and temperature of the current source 1 becomes

$$R_{eq,1} = R_r + R^{(1)}_{d(1)} || R_{d(2)} || \cdots || R_{d_{(2n)}}$$
$$T_1 = R_{eq,1} \cdot Q/2n \quad (17)$$

The equivalent thermal resistance at branch 2 can be solved by similar principles. And most of lumped resistances in (7) can be reused over here except $R^{(2)}_{d(2)}$ which needs to be evaluated

independently.

$$R_{eq,2} = R_r + R_{d(2n)}||R^{(2)}_{d(2)}||R_{d(3)}||\cdots||R_{d_(2n)} \qquad T_2 = R_{eq,2} \cdot Q/2n \quad (18)$$

Therefore, the general equivalent thermal resistance and temperature seen from the heat source of branch i becomes

$$R_{eq,i} = R_r + R_{d(2n)}||R_{d_(2n-1)}||\cdots||R_{d_(2n-i+1)}||R^{(i)}_{d(i)} \\ ||R_{d(i+1)}||\cdots||R_{d(2n)} \quad T_i = R_{eq,i} \cdot Q/2n \quad (19)$$

With the equivalent thermal resistance and temperature at each heat source, the average equivalent thermal resistance and temperature of the winding block surface is

$$R_{eq,avg} = R_r + \frac{1}{n}\sum_{i=1}^{n} R_{eq,i} \quad T_{avg} = R_{eq,avg}Q/2n \quad (20)$$

The overall average equivalent thermal conductivity can be evaluated with average temperature rise, litz wire block dimensions, and heat flux.

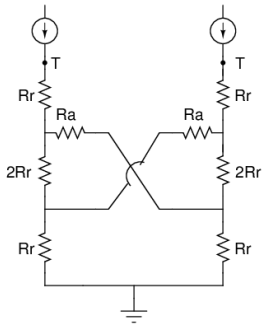

Fig. 9: Simplified Model of the Proposed Litz Wire

2) Simplified Model: For a quick prediction of equivalent thermal conductivity, its associated thermal equivalent circuit can by simplified as $n = 1$. Also, the curvature portion is assumed not to conduct heat radially. Therefore, the corresponding lumped thermal resistance circuit is displayed in Fig. 9. Only two element thermal resistances need to be evaluated here, R_a and R_r:

$$Ra = 2(\frac{L\sec\theta - 2H\csc\theta}{n \cdot WHk_{b,a} \cdot ff} + \frac{\csc\theta}{Wk_{b,a} \cdot ff}) \quad (21)$$

$$Rr = \frac{n \cdot H}{W(L\sec\theta - 2H\csc\theta)} \frac{k_f}{k_{b,r}} \frac{(1+ff)k_{b,r} + (1-ff)k_f}{(1-ff)k_{b,r} + (1+ff)k_f} \quad (22)$$

By applying superposition principle and circuit manipulation techniques, the equivalent total thermal resistance associated with one heat source is simplified as

$$R_{tot} = 2R_r \cdot \frac{(10R_r^2 + 11R_rR_a + 2Ra^2)}{2R_r^2 + 8R_rR_a + R_a^2} \quad (23)$$

And the equivalent thermal conductivity of potted litz wire with transposition arrangement can be obtained from total resistance:

$$k_e = \frac{H}{W(L\sec\theta - 2H\csc\theta)R_{tot}} \quad (24)$$

This simplified model combined with bundle homogenization equations can be easily implemented in MATLAB and excel sheet. It can also facilitate machine design optimization and electro-thermal trade-off study.

IV. Validation Results

This section presents a detailed 3-D FEA model of transposed litz wire to validate analytical model results. Both bundle radial and axial thermal conductivity were varied in a large range to confirm the proposed analytical model prediction accuracy. Furthermore, litz wire with parallel arrangement was modeled to explore the benefits of using transposition arrangement from thermal aspect. At last, a hardware setup was used to validate prediction values using the selected litz wire samples that is potted within resin.

A. 3-D FEA Simulation

The 3-D model for the rectangular transposed litz wire was imported into ANSYS to simulate steady state thermal analysis. Only one pitch of transposed wires are modeled and calculated. The bundles within resin block are assigned with radial and axial thermal properties and local coordinates. The bottom boundary condition of resin block is 20 C. The top boundary condition of resin block is 50 W heat applied. Other boundary surfaces are assigned with perfect insulation. The parallel arrangement was also modeled to study transposition effects on litz wire thermal conductivity. The resin and litz wire bundle radial and axial thermal conductivity are assigned with specific values that are close to the real case in Section II.

Figure 10 and 11 are the temperature distribution contours of transposed and parallel litz wire. It is interesting to notice that temperature rise in transposed case is lower than the parallel case, since bundles have large thermal conductivity on axial (transverse) direction. The hotspot temperature of the potted litz wire block with transposition is around 10.5% lower than the parallel one. And the maximum temperature on the liz wire bundle of transposition bundle is 15.5% lower than the parallel one. Even though the bundle radial thermal conductivity is only 0.88% of the axial thermal conductivity, the axial dimension of litz wire bundle is hundred times than the radial dimension, which reduces thermal benefits using transposition arrangement.

B. Theory and Simulation Prediction Comparison

The effective thermal conductivity of the simulated transposed litz wire dimensions are calculated using equations in III. The boundary conditions, litz wire geometry, and material properties are the same in both calculation and simulation setup of IV-A. The theoretical and simulation prediction results were compared with varying both bundle radial and axial thermal conductivities in wide ranges. Such way can better

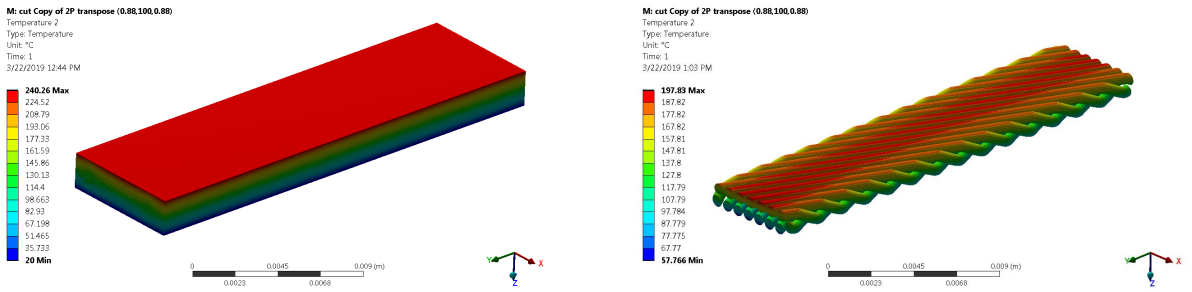

(a) Resin Block (b) Litz Wire

Fig. 10: Simulation Results for the Transposed Arrangement ($k_{bundle,r} = 0.88W/mK, k_{bundle,a} = 100W/mK, k_{resin} = 0.8W/mK$)

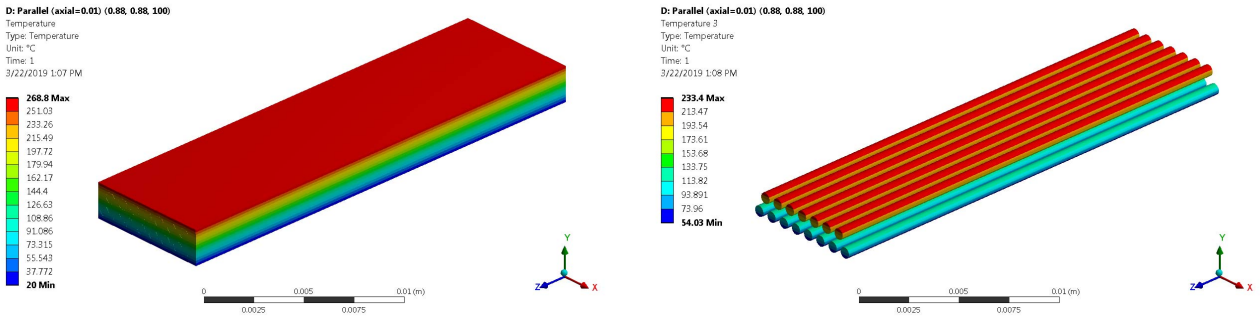

(a) Resin Block (b) Litz Wire

Fig. 11: Simulation Results for the Parallel Arrangement ($k_{bundle,r} = 0.88W/mK, k_{bundle,a} = 100W/mK, k_{resin} = 0.8W/mK$,)

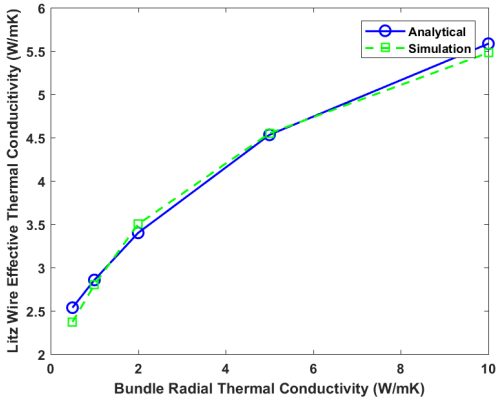

Fig. 12: Analytical Model Validation with Various Bundle Radial Thermal Conductivity

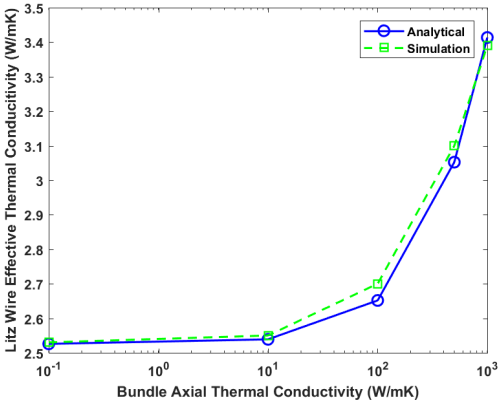

Fig. 13: Analytical Model Validation with Various Bundle Axial Thermal Conductivity

capture transposition effects on litz wire heat dissipation performance.

Figure 12 presents the effective thermal conductivity results of both theoretical and simulation by varying bundle radial (perpendicular) thermal conductivity from 0.5 - 10 W/mK. The axial thermal conductivity is fixed as 100 W/mK here. The simulation result is based on average temperature of the top surface. Even though there is a uniform heat flux boundary condition applied, the temperature rise distribution across litz wire is not the same everywhere. Because copper and insulation distributions are not uniform along x,y,z directions in the transposed. The litz wire with parallel arrangement has

TABLE II: Experimental Data of Three Samples

Windings	Thickness [mm]	Area [mm^2]	Qin [W]	Qout [W]	T [C]	Rtotal [K/W]	Rsample [K/W]	Ksample [W/mK]
sample1	5.6	6.8 X 25.4	1.0805	0.9677	36.77	35.90	28.83	1.124
sample2	11.45	6.8 X 25.5	0.7549	0.6926	42.72	59.02	51.95	1.276
sample3	17.3	6.8 X 25.6	0.5533	0.5353	50.37	92.54	85.46	1.171

uniform material distribution along with axial direction. Figure 13 shows the effective thermal conductivity of various bundle axial thermal conductivity values while fixing bundle radial thermal conductivity as 0.88 W/mK. The variation of bundle axial thermal conductivity is large ranging from 0.1 - 1000 W/mK. Both Fig. 12 and 13 show that the theoretical results have a good agreement with the simulation results by varying both radial and axial thermal properties.

Regarding computational time, using analytical model to predict effective thermal conductivity only costs 1-2 seconds in MATLAB programming environment. However, simulation model needs at least half hour to finish meshing and computational process. If CAD model development is included, simulation model will cost days to months work. Overall, the proposed analytical model, especially simplified model has advantages of saving computation time and working efforts.

C. Theoretical and Experimental Results Comparison

There are three samples used during the equivalent thermal conductivity measurement test. All of these samples were made with the same type of litz wire presented in Section II. Sample 1 has three layers of litz wire and potted with epoxy resin. Sample 2 has six layers and sample 3 has 12 layers. The associated material properties are listed in Table I.

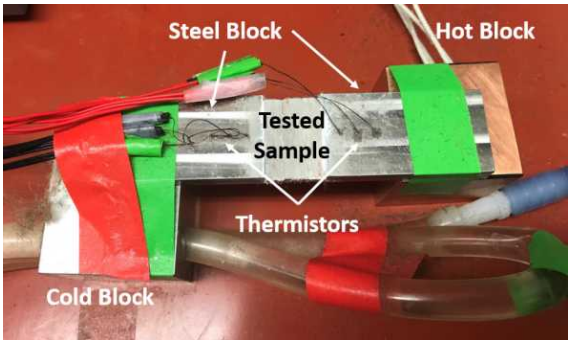

Fig. 14: Equivalent Thermal Conductivity Measurement Setup

The equivalent thermal conductivity measurement setup was initially designed for measuring thermal switch property [15]. It consists of cold and hot copper block and steel interface blocks drilled with three thermistor holes respectively. The hot copper block is supplied with consistent heat source generated by a dc power supply. The cold copper block is cooled by chiller water which is set with 10 C. Two pieces of steel interface blocks were manufactured with the exact same interface area as the ones of sample blocks. Sample was inserted between two steel blocks and covered with thermal paste to minimize thermal contact resistance. Furthermore, temperature was measured through six thermistors, not popular thermocouples. Because thermistors have more stable and accurate temperature measurement. All of thermistors were located with 5 mm gap shown in Fig 14. Insulation foam was wrapped around the setup to minimize heat flux leaking from thermal conduction process.

The temperature measurements were collected at steady state where temperature difference stays within 0.1 C. The sample dimensions, heat source, and temperature measurements are presented in Table II. The effective thermal conductivity of three samples have similar values. The average value of the selected litz wire effective thermal conductivity is 1.188 W/mK. And the analytical prediction of equivalent thermal conductivity using Section III is 1.1 W/mK. So the prediction value has roughly 8% error. It indicate that the presented analytical model is effective in predicting litz wire equivalent thermal conductivity considering transposition.

V. Conclusions

Transposition effects on equivalent thermal conductivity of potted litz wire are studied in this paper. A detailed analytical model of predicting transposed litz wire thermal performance is presented and discussed. Simulation and hardware experiments are used to validate the proposed prediction method accuracy. It turns out that the proposed analytical model prediction has a good agreement with both validation results.

References

[1] X. Zhang, C. L. Bowman, T. C. O'Connell, and K. S. Haran, "Large electric machines for aircraft electric propulsion," *IET Electric Power Applications*, vol. 12, no. 6, pp. 767–779, jul 2018.

[2] M. Popescu, D. A. Staton, A. Boglietti, A. Cavagnino, D. Hawkins, and J. Goss, "Modern Heat Extraction Systems for Power Traction MachinesA Review," *IEEE Transactions on Industry Applications*, vol. 52, no. 3, pp. 2167–2175, may 2016.

[3] A. A. Woodworth, R. Jansen, K. Duffy, P. N. Author, and E.-S. Shin, "Creating a multifunctional composite stator slot material system to enable high power density electric machines for electrified aircraft applications."

[4] J. Martin, A. Yoon, A. Jin, and K. S. Haran, "High-Frequency Litz Air-Gap Windings for High-Power Density Electrical Machines," *Electric Power Components and Systems*, vol. 45, no. 7, pp. 798–805, apr 2017.

[5] C. R. Sullivan and R. Y. Zhang, "Simplified design method for litz wire," in *2014 IEEE Applied Power Electronics Conference and Exposition - APEC 2014*. IEEE, mar 2014, pp. 2667–2674.

[6] X. Yi, A. Yoon, and K. S. Haran, "Multi-physics optimization for high-frequency air-core permanent-magnet motor of aircraft application," in *2017 IEEE International Electric Machines and Drives Conference (IEMDC)*. IEEE, may 2017, pp. 1–8.

[7] H. Liu and J. Hahne, "High-speed compulsator stator thermal management," *IEEE Transactions on Magnetics*, vol. 39, no. 1, pp. 357–361, jan 2003.

[8] X. Huang, Q. Tan, L. Li, J. Li, and Z. Qian, "Winding Temperature Field Model Considering Void Ratio and Temperature Rise of a Permanent Magnet Synchronous Motor with High Current Density," *IEEE Transactions on Industrial Electronics*, 2016.

[9] A. Boglietti, M. Cossale, S. Vaschetto, and T. Dutra, "Thermal Conductivity Evaluation of Fractional-Slot Concentrated-Winding Machines," *IEEE Transactions on Industry Applications*, vol. 53, no. 3, pp. 2059–2065, may 2017.

[10] R. Wrobel, S. Ayat, and J. L. Baker, "Analytical methods for estimating equivalent thermal conductivity in impregnated electrical windings formed using Litz wire," *2017 IEEE International Electric Machines and Drives Conference, IEMDC 2017*, 2017.

[11] N. Simpson, R. Wrobel, and P. H. Mellor, "Estimation of equivalent thermal parameters of impregnated electrical windings," *IEEE Transactions on Industry Applications*, 2013.

[12] P. Romanazzi, M. Bruna, and D. A. Howey, "Thermal Homogenization of Electrical Machine Windings Applying the Multiple-Scales Method," *Journal of Heat Transfer*, vol. 139, no. 1, p. 012101, 2016.

[13] M. Jaritz, A. Hillers, and J. Biela, "General Analytical Model for the Thermal Resistance of Windings Made of Solid or Litz Wire," *IEEE Transactions on Power Electronics*, 2018.

[14] N. J. Renner, J. D. Lenz, X. Yi, and K. S. Haran, "Development of form-wound air-core armature windings for high-frequency electric machines," in *2017 IEEE International Electric Machines and Drives Conference (IEMDC)*. IEEE, may 2017, pp. 1–8.

[15] T. Yang, B. Kwon, P. B. Weisensee, J. G. Kang, X. Li, P. Braun, N. Miljkovic, and W. P. King, "Millimeter-scale liquid metal droplet thermal switch," *Applied Physics Letters*, vol. 112, no. 6, p. 063505, feb 2018.